Spatial current-density instabilities in multilayered semiconductor structures

A. V. Gorbatyuk
A.F. Ioffe Physicotechnical Institute, Russian Academy of Science, Politekhnicheskaya 26, 194021 St. Petersburg, Russia

F.-J. Niedernostheide
Institut für Angewandte Physik, Universität Münster, Corrensstraße 2/4, 48149 Münster, Germany, and Infineon AG, Balanstr. 59, 81541 München, Germany

(Received 15 November 2001; published 18 June 2002)

Semiconductor p^+-p^--n-p^+-n^{++} structures are considered as (1×2)-dimensional active media. Such systems may exhibit several carrier injection modes associated with different nonequilibrium plasma/field patterns along the cathode-to-anode direction and numerous self-organized current-density patterns in the transversal plane. We study a peculiar field punch-through (FPT) mode by regarding the structure to be composed of two transistor subsystems coupled by a field domain. The suggested model allows one to analyze the stability properties of the uniform FPT mode with respect to transversal harmonic perturbations of the distributed variables. An analysis of the dispersion relations $\zeta(k)$ shows that depending on the material and design parameters three different types of instability may occur. The first one is of Ridley type, in which ζ first becomes positive for the lowest wave number $k\to0$. The second case corresponds to an analog of Turing's instability where the uniform state is destabilized by a fluctuation with a wave number $k>0$ and being different from the lowest possible k value. Third, at certain conditions both types of instability may appear simultaneously, so that a new diversity of spatiotemporal patterns can be expected due to the competition between fluctuations with different wave numbers.

DOI: 10.1103/PhysRevB.65.245318 PACS number(s): 72.20.Ht, 05.45.−a, 85.30.−z

I. INTRODUCTION

Studies of current-density instabilities in self-organizing solid-state media based on multilayered semiconductor structures are motivated by two factors. First, they are aimed at a deeper understanding of self-organized patterns, their evolution and properties and the general concepts of self-organization.[1–5] Second, such multilayered structures seem attractive for certain applications as, e.g., neural algorithms[6,7] or image processing systems[8,9] in semiconductor device technology. For such kinds of applications, the exploitation of propagating fronts, stationary or traveling current-density filaments, and spatially periodic current-density patterns are very promising. Although, e.g., current-density filaments may appear in diverse semiconductor systems as n GaAs,[10–14] p Ge,[15] Si p-n diodes,[16,17] Si multilayered devices,[18–20] or ac-driven thin-film ZnS:Mn devices,[21,22] Si multilayered structures are advantageous because of the well-developed silicon technology, the room-temperature operation of the device and the variety of patterns which have already been observed in these structures. While instabilities in thyristors are usually connected with a pronounced negative differential resistance (NDR) and can often be attributed to an instability of Ridley type,[23] there are also indications of Turing-like patterns[1] in thyristorlike structures[18] and in Si thyristors[24–26] under certain conditions. Furthermore, interesting dynamics of switching fronts have been predicted in gate-driven p-n-p-n structures,[27,28] while in p^{++}-n^+-p-n^--n^+ structures various generic types of filament oscillation have been observed, including pendulumlike filament oscillations[19,29] and traveling[18,30] and spiking filaments.[31]

The present paper is a continuation of experimental and theoretical studies[18,32–34] of thyristorlike systems with a specific multilayer p^+-p^--n-p^+-n^{++} structure. In Refs. 33 and 34 we theoretically studied the nature of possible local trigger mechanisms in p^+-p^--n-p^+-n^{++} structures in detail. They were based on a double-injection process coupled with a positive current feedback loop between electron and hole injection currents. However, depending on the design parameters two basically different situations can occur, leading to different instability scenarios.

If the efficiency of the n^{++}-p^+ electron emitter is large enough, local switching is possible at relatively low and moderate currents. If, additionally, the excess carrier lifetime in the bulk is small, a plasma layer $\mathcal{P}$ may evolve in the p^- bulk close to the p^--n junction. In this case, the p^+-p^--n-p^+-n^{++} structure can be considered to be composed of two interactive subsystems: a thyristorlike active subsystem, the $\mathcal{P}$-n-p^+-n^{++} subsystem, and a passive resistive layer (the p^+-p^- subsystem). Based on this concept, a (1×2)-dimensional analytical approach was developed.[34] An analysis of the derived model equations showed that, depending on the device parameters, the stationary homogeneous current-density state may be destabilized by a mechanism of either Ridley[23] or Turing[1] type.

If, in contrast, the injection efficiency of the electron emitter is sufficiently small, which occurs if the doping concentration of both the n^{++} and p^+ layers is sufficiently high, the space-charge region of the reversely biased p^+-n junction can totally occupy the n base, and furthermore the field domain can expand over the main part of the low-doped p^- bulk of the structure. After this, the n base no longer exists more as a functional element of the thyristorlike subsystem. Nevertheless, as shown in Ref. 33, both theoretically and by measurements, a thyristorlike regenerative trigger mecha-

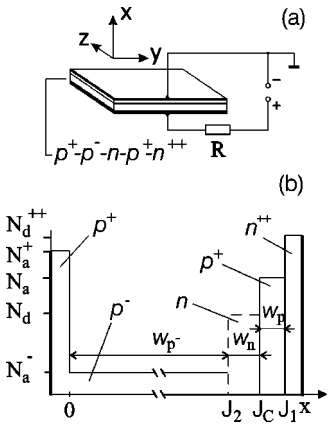

FIG. 1. Geometry of the sample (a) and doping profile along the (anode-to-cathode) x direction (b).

nism may appear under these conditions. In this case, the p^+-p^--n-p^+-n^{++} structure can be divided into p^+-$\mathcal{P}$-$\mathcal{F}$ and $\mathcal{F}$-p^+-n^{++} subsystems, acting as a virtual anode and a cathode transistor, respectively, and coupled by a field domain $\mathcal{F}$ covering the residual part of the p^- bulk and the whole n layer.[33] The field domain $\mathcal{F}$ works as a collector in both virtual transistors and the plasma layer $\mathcal{P}$ acts as a base in the anode transistor. We refer to this type of injection mode as field punch-through mode (FPT mode).

In the FPT mode the total depletion of the n layer essentially changes the functions of the subsystems; thus we expect a drastic modification of the transversal instability mechanism in comparison with the cases studied earlier.[34] In particular, the conductivity modulation of the field domain and the fact that its anode-side boundary, the $\mathcal{P}$-$\mathcal{F}$ boundary, is floating should cause a variety of peculiarities concerning the evolution of transversal current-density and potential fluctuations.

In this paper we therefore suggest an analytical approach for the instability mechanism in the family of p^+-p^--n-p^+-n^{++} structures operating in the FPT mode. The paper is organized as follows. In Sec. II the investigated semiconductor structure is described and the regenerative thyristorlike mechanism of the FPT mode is explained. An adequate (1×2)-dimensional analytical theory is developed in Sec. III. The stationary homogeneous states are determined in Sec. IV, and the dispersion relations are derived in Sec. V. In Sec. VI several limit cases are discussed, illustrating the influence of the transversal currents in the transistor subsystems and the potential fluctuations in the field domain on the stability properties of the whole system. Finally, typical instability scenarios arising in the multilayered structure are presented and conditions for the simultaneous appearance of Ridley- and Turing-type instability are derived.

II. SEMICONDUCTOR STRUCTURE AND FIELD PUNCH-THROUGH MODE

The multilayer structure under consideration is a p^+-p^--n-p^+-n^{++} structure with large contact areas [Fig. 1(a)] driven by dc bias V_S via a load resistor R. For simplicity a stepwise doping profile [Fig. 1(b)] is assumed, approximating the experimentally investigated structure described in detail in Refs. 18 and 32. The design topology in the vertical direction can qualitatively be characterized by the relations

$$w_p, w_n \ll w_{p^-}, \quad N_a \gg N_d > N_a^-, \tag{1}$$

where w_{p^-}, w_n, and w_p denote the widths of the p^- bulk, the n base, and the p^+ base, respectively, and N_a^-, N_d, and N_a their corresponding doping concentrations. The excess carrier lifetime τ inside the p^- bulk is assumed to be of the order of ~ 10 μs. In the doped layers, especially in the p^+ base, the lifetime τ_1 is at least one order of magnitude lower because of the well-known heavy doping effects.

In equilibrium there are three p-n junctions, namely J_1, J_C, and J_2, formed by the n^{++}-p^+, the p^+-n, and n-p^- junctions, respectively. At a small forward bias ("+" at the p^+ emitter) the junctions J_1 and J_2 play roles of electron and hole emitters, while J_C acts as a collector, similar to thyristorlike systems described in Ref. 34.

For the realization of the FPT mode at larger biases the doping profile is subjected to certain restrictions. The first one concerns the doping concentrations of the n^{++} emitter and the p^+ base which should be in such a relation that the emitter efficiency γ_1 of the junction J_1 is sufficiently small,

$$\gamma_1(j_1) = \frac{j_{1n}}{j_1} < a_h = \frac{b}{b+1}, \tag{2}$$

where j_1 and j_{1n} denote the total emitter current density and the electron emitter current density, respectively, and $b = \mu_n/\mu_p$ is the electron-to-hole mobility ratio. Physically, Eq. (2) means that the injected electron current never exceeds the electron drift current under high injection conditions.

The second restriction concerns the parameters of the inner n layer. When the forward bias is increased, the space-charge region of the junction J_C, subsequently called the high-field domain $\mathcal{F}_h$, expands into the n layer toward the junction J_2. If the doping concentration N_d and the width w_n of the n layer satisfy the inequality

$$N_d w_n < \frac{\epsilon\epsilon_0 E_{av}}{q}, \tag{3}$$

it can be ensured that the maximum electric field remains below the avalanche breakdown field E_{av} ($\sim 2\times10^5$ V/cm in silicon) even when the anode-side boundary of the high-field domain $\mathcal{F}_h$ reaches the junction J_2. Here q, ϵ_0, and ϵ denote the elementary charge, the vacuum permittivity, and the dielectric constant of the material. During this phase the diffusion current of holes injected from the p^- bulk passing the quasineutral part of the n base and the field domain $\mathcal{F}_h$ causes an increase in the electron injection of the junction J_1. The total current density is, however, strictly limited by the large resistance of the p^- bulk.

As the voltage increases further, the current density j may significantly exceed the characteristic equilibrium current density $j_{D_{eq}}$ of the junction J_2, and is therefore mainly carried by a field current

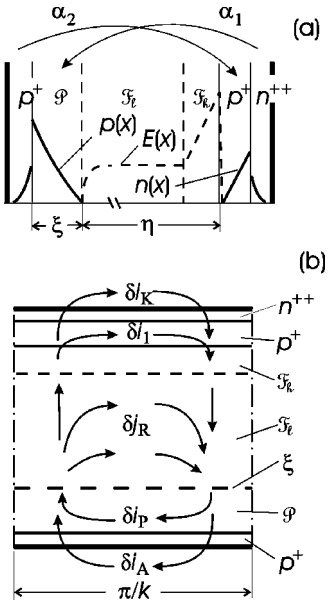

FIG. 2. Nonequilibrium plasma-field stratification along the vertical direction (a) and possible contours of small current-density fluctuations, which are periodical along the transversal direction **r** (b).

$$j \gg j_{D_{eq}} \sim \frac{qDN}{\lambda_D},$$

and the quasineutral part of the n layer may completely vanish. Here $\lambda_D = \sqrt{\epsilon\epsilon_0 kT/q^2 N}$ is the Debye length, and N denotes the characteristic free carrier concentration. For smooth junctions N is of the order of the doping concentration at the position x, where the donor concentration is equal to the acceptor concentration; in the considered case we have $N \approx N_a^-$. Thus a total field punch-through of the n layer occurs, when the space-charge region, i.e., the high-field domain $\mathcal{F}_h$, occupies the whole width w_n. The punch-through threshold voltage is defined as

$$V_{pth} = \frac{qN_d w_n^2}{2\epsilon\epsilon_0}. \tag{4}$$

For further consideration, the voltage range $V > V_{pth}$ (the FPT mode) is of main interest. The FPT mode is characterized by a specific plasma/field stratification along the vertical x direction [Fig. 2(a)]. While the field domain expands as a low-field domain $\mathcal{F}_l$ into the p^- bulk from the cathode side, a plasma layer $\mathcal{P}$ with an increased carrier concentration develops inside the p^- bulk close to the anode side p^+ contact. The width ξ of this $\mathcal{P}$ layer is assumed to be smaller than the diffusion length $L_h = (D_h \tau)^{1/2}$, and therefore satisfies the inequality

$$\xi \ll (D_h \tau)^{1/2} < w_{p^-}. \tag{5}$$

As shown in Ref. 33, if $\gamma_1(j_1) < a_h$ [Eq. (2)], the $\mathcal{P}$ layer has a sharp boundary with the low-field domain $\mathcal{F}_l$. The excess carrier concentration in $\mathcal{F}_l$ remains relatively small, and ambipolar drift transport predominates over diffusion at sufficiently low fields. The p^+ emitter, the $\mathcal{P}$ layer, and the field domain $\mathcal{F} = \mathcal{F}_l + \mathcal{F}_h$ form a functional element working as virtual p^+-$\mathcal{P}$-$\mathcal{F}$ transistor, subsequently called the anode-side transistor T_A.

The interaction between the anode-side transistor T_A and the cathode-side thyristor T_K, the n^{++}-p^+-$\mathcal{F}$ transistor, is manifested in the condition[33]

$$\alpha_1(j) + \alpha_2(j,V) = 1, \tag{6}$$

holding for stationary homogeneous states in thyristorlike devices.[35,36] Here α_1 and α_2 denote the current gains of the transistors T_K and T_A, respectively [Fig. 2(a)], and V is the voltage drop across the whole multilayer structure. Only if at least one of the two coefficients increases with current, a thyristorlike regeneration process and a range of NDR in the stationary current-density vs voltage characteristic $j(V)$ may appear. Such dependencies of the current gains can be provided by different nonlinear recombination mechanisms[35,36] which lead to emitter leakage currents depending sublinearly on the injection current. In practice, the desired dependencies of $\alpha_1(j)$ and $\alpha_2(j)$ can be adjusted by utilizing special distributed gridlike shunts or even driving gate elements tailoring the efficiency of the emitter junctions.[37] In the following, it is supposed that suitable sublinear leakage mechanisms exist in both transistor subsystems.

The low-field domain $\mathcal{F}_l$ contributes essentially to the voltage drop across the p^- bulk. It should be noted that the internal n layer, when totally depleted, does not play any active role for the regeneration process, in contrast to the situation considered in Ref. 34. The FPT mode can even be realized without it (i.e., without the development of the high-field domain $\mathcal{F}_h$). Nevertheless, the existence of the $n/\mathcal{F}_h$ layer influences the shape of the $j(V)$ characteristic, and therefore changes the triggering characteristic quantitatively.

The stability properties of the homogeneous FPT mode may be influenced by small nonuniform current-density fluctuations. Figure 2(b) schematically illustrates various contours of possible current fluctuations resulting from the specific (1×2)-dimensional configuration of the structure. Obviously, the current paths may lead partly vertically across the individual layers and partly transversally along the doped layers, the metal contacts or the high-resistivity p^- bulk in the $\boldsymbol{r}$ direction, $\boldsymbol{r} = \boldsymbol{y} + \boldsymbol{z}$. These current fluctuations are inseparably linked with corresponding fluctuations of the carrier concentration, the electric field, and the potential and with fluctuations of the boundary position between the plasma layer $\mathcal{P}$ and the field domain $\mathcal{F}$.

III. (1×2)-DIMENSIONAL MODEL

In this section we develop the physical description of the two transistor subsystems and the field domain coupling the two subsystems. After that the time scale hierarchy is discussed and finally a self-consistent (1×2)-dimensional set of model equations is derived.

A. Transistor T_A

It is convenient to characterize the excitation conditions for quasineutral elements of the system by the injection level, i.e., the ratio between the excess carrier concentration and the doping concentration. The FPT mode is characterized by a high injection level in the $\mathcal{P}$ layer of the transistor T_A.

The charge dynamics in T_A can be described in terms of the well-known charge-control model.[35] According to this approach we consider the specific charge density $Q(y,z,t) = Q(\boldsymbol{r},t)$ per unit square of the plasma layer $\mathcal{P}$ in T_A,

$$Q(\boldsymbol{r},t) = q \int_{\xi(\boldsymbol{r},t)} p(x,t)\,dx, \tag{7}$$

where $p(x)$ is the excess carrier concentration along the width ξ of the virtual $\mathcal{P}$ base.

By assuming quasineutrality in the virtual base the local dynamics of this charge for the two-dimensional transversal geometry can be described by

$$\frac{\partial Q}{\partial t} = D_\perp \Delta_\perp Q - \frac{Q}{\tau} + j_{\xi n} - j_{lk}. \tag{8}$$

Here $\Delta_\perp = \partial^2/\partial y^2 + \partial^2/\partial z^2$ is the two-dimensional Laplace operator, $D_\perp$ an effective diffusion coefficient, τ the excess carrier lifetime at high injection levels, $j_{\xi n}$ the normal component (along the x direction) of the electron current density at the boundary between the $\mathcal{P}$ layer and the low-field domain $\mathcal{F}_l$, j_{lk} the current density of electrons leaving the $\mathcal{P}$ layer at the p^+-$\mathcal{P}$ junction by leakage mechanisms which will be discussed below. Under high injection conditions the hole injection current density at this boundary consists of a drift and a diffusion current density, whereby the first one is determined by the electron-to-hole mobility ratio b and the second one depends on the stored charge Q in the $\mathcal{P}$ layer and the diffusion transit time θ,

$$j_{\xi p} = \frac{1}{b+1} j_\xi + \frac{Q}{\theta}, \tag{9}$$

$$\theta(\xi) = \frac{\xi^2}{2D_h}, \tag{10}$$

where $D_h = 2D_p b/(b+1)$ is the ambipolar diffusion coefficient and D_p denotes the hole diffusion coefficient.

Taking into account that the total current j_ξ at the $\mathcal{P}$-$\mathcal{F}$ junction is given by $j_\xi = j_{\xi p} + j_{\xi n}$, Eq. (9) can be rewritten

$$Q = j_\xi g\,\theta, \tag{11}$$

$$g = a_h - a(j_\xi, j_{\xi n}) > 0, \tag{12}$$

where $g > 0$ always holds because of Eq. (2).

Furthermore we assume, that the electron leakage current density j_{lk} at the p^+-$\mathcal{P}$ plane is determined by the excitation level in the vicinity of this plane which in turn can be estimated from the maximum value of the excess plasma concentration Δp_m in the $\mathcal{P}$ layer:

$$\Delta p_m \simeq \frac{2Q}{q\xi}. \tag{13}$$

We consider two different groups of leakage mechanisms. The respective current densities j_{sb} and j_{sp} depend sublinearly and superlinearly on the plasma charge Q. The total leakage current j_{lk} is then given by

$$j_{lk} = j_{sb} + j_{sp}. \tag{14}$$

The sublinear leakage components suppress the hole injection at low injection levels and may emanate from recombination rates decreasing with the current, or from intentionally incorporated microdistributed shunts as mentioned in Sec. II. We will account for different mechanisms by the phenomenological term

$$j_{sb} = C_{sb}^{(\nu)} \left(\frac{Q}{\xi} \right)^\nu, \quad \nu < 1, \tag{15}$$

where $C_{sb}^{(\nu)}$ is a ν-dependent proportionality factor. For higher current density values the dependence of j_{sb} on Q becomes very weak. If, e.g., emitter shunts with a finite shunt resistance R_{sh} are used, the leakage current is limited by the value $V_A^{\max}/R_{sh}$, where $V_A^{\max}$ is the maximum voltage drop (typically $\leqslant 1$ V) across the shunted junction. Therefore, j_{sb} practically saturates at a constant value, a fact which is used for an estimation below.

At high injection levels the injection efficiency is limited due to Fletcher's mechanism,[38] smooth doping effects,[39] Auger recombination,[40] etc. These effects cause extra carrier losses adding to the usual recombination processes; they are described here by the following term showing a superlinear dependence on the plasma charge Q:

$$j_{sp} = C_{sp}^{(\mu)} \left(\frac{Q}{\xi} \right)^\mu, \quad \mu > 1, \tag{16}$$

with the μ-dependent proportionality factor $C_{sp}^{(\mu)}$. If only Fletcher's mechanism is limiting the injection efficiency, we have $\mu = 2$ and, in accordance with Ref. 33, $C_{sp} = 4D_n/q\lambda_{eff}N_a^+$, where N_a^+ and λ_{eff} denote the doping concentration and the effective diffusion length of electrons in the p^+ layer, respectively, and D_n is the electron diffusion coefficient. The relations between the total current density j_ξ and the electron current density $j_{\xi n}$ are governed by processes in the transistor T_K and the field domain $\mathcal{F}$, which are considered in more detail in the following two subsections.

B. Transistor T_K

The transistor subsystem T_K has a vertical doping profile which resembles that for high-frequency transistors, and can be described in terms of Shockley's junction theory (see, e.g., Ref. 36). The injection level in the p^+ base can be characterized by the minority excess concentration Δn, and is assumed to be relatively low, $\Delta n \sim \exp(q\varphi_1/kT) \ll N_a$, where φ_1 denotes the voltage drop across the junction J_1. Accordingly, in this case the vertical component of the current density is governed by diffusion of electrons injected

into the p^+ base, while the transversal current consists only of a hole drift current $i_1 \sim -\nabla_\perp \varphi_1$. Here $\nabla_\perp = (\partial/\partial y, \partial/\partial z)$ is the two-dimensional ∇ operator.

The continuity equation describing the local charge dynamics in the p^+ base can be written in the form

$$C_{1e}(\varphi_1)\frac{\partial \varphi_1}{\partial t} = \sigma_1 w_p \Delta_\perp \varphi_1 + j_C - j_1, \tag{17}$$

where C_{1e} denotes the voltage dependent capacitance per unit square of the junction J_1 and $\sigma_1 = q\mu_p N_a$ is the conductivity of the p^+ base. The terms $j_C = j_{Cn} + j_{Cp}$ and $j_1 = j_{1n} + j_{1p}$ are the vertical components of the current density at the $\mathcal{F}$-p^+ junction and the junction J_1, respectively, where the index n (p) denotes the electron (hole) component. The electron injection current density j_{1n} of the junction J_1 can be expressed by $j_{1n} = j_{n0}\ [\exp(q\varphi_1/kT) - 1]$, which implies a linear dependence on the excitation level. Here and below, saturation current densities[36] are denoted by $j_{\ldots 0}$. The hole leakage current density j_{1p} may consist of both linear and sublinear parts: $j_{1p} = j_{lin} + j_{sub}$. The linear component is due to hole diffusion into the n^{++} layer: $j_{lin} = j_{p0}[\exp(q\varphi_1/kT) - 1]$. The sublinear component may occur due to Sah-Noyce-Shockley recombination or the excess current density component of a tunnel current.[33,34] In both cases j_{sub} is of the form $j_{sub} = j_{sb0}[\exp(A\varphi_1) - 1]$ with $A < q/kT$, and therefore, $j_{sub} \sim (j_n)^{\nu_1}$ with $\nu_1 = AkT/q < 1$.

The capacitance $C_{1e}(\varphi_1) = C_B + C_D$ consists of the barrier capacitance $C_B \sim [(q\epsilon\epsilon_0 N_a)/2(\varphi_b - \varphi_1)]^{1/2}$ and the diffusion capacitance $C_D = q j_{1n}\theta_1/kT$, where φ_b is the built-in potential, and $\theta_1 = w_p^2/2D_n$ denotes the p^+ base transit time. The values of C_B and C_D are considered to be of the same order for the junction J_1.

Finally, the current density j_1, its electron component j_{1n}, and the electron injection coefficient γ_1 of the cathode emitter can be expressed as function of the emitter voltage φ_1:

$$j_1(\varphi_1) = (j_{n0} + j_{p0})[\exp(q\varphi_1/kT) - 1] + j_{sb0}[\exp(A\varphi_1) - 1], \tag{18}$$

$$j_{1n}(\varphi_1) = j_{n0}[\exp(q\varphi_1/kT) - 1], \tag{19}$$

$$\gamma_1(j) = \frac{j_{1n}}{j_1} = \gamma_1(\varphi_1). \tag{20}$$

Because of the sublinear character of j_{sub} as function of electron current density j_{1n}, the coefficient γ_1 saturates at sufficiently large current densities, provided that the low injection condition is not violated.

C. Virtual collector

In the high-field part $\mathcal{F}_h$ of the field domain, the concentrations of free carriers are negligibly small, $n, p \ll N_d$; therefore, Poisson's equation is given by

$$\Delta\varphi = -\frac{qN_d}{\varepsilon\varepsilon_0}, \tag{21}$$

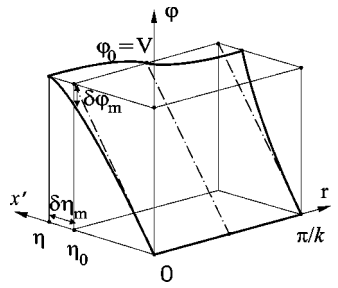

FIG. 3. Potential distribution $\varphi(x', \mathbf{r})$ illustrating the correlation between potential fluctuations $\delta\varphi$ and fluctuations $\delta\eta$ of the anode-side boundary of the field domain.

where $\Delta = \partial^2/\partial x^2 + \partial^2/\partial y^2 + \partial^2/\partial z^2$ is the three-dimensional Laplace operator, and the electric-field strength follows from

$$\boldsymbol{E} = -\nabla\varphi. \tag{22}$$

In Ref. 33 we showed that the low-field domain $\mathcal{F}_l$ has a sharp boundary with the plasma $\mathcal{P}$ layer and its main part is quasineutral. Therefore, in the low-field domain $\mathcal{F}_l$ the Poisson equation simplifies to

$$\Delta\varphi = -\frac{q}{\varepsilon\varepsilon_0}(p - n - N_a^-) = 0. \tag{23}$$

At the boundary $x' = w_{p^-} + w_n - x = w_n$ between the low- and high-field domains the x component E_x of the electric field satisfies the condition

$$E_x|_{x' = w_n - 0} = E_x|_{x' = w_n + 0}. \tag{24}$$

Since the voltage drops of the emitter junctions are relatively small (typically $\leqslant 1$ V), we assume that the voltage V applied to the multilayer structure completely drops across the field domain, i.e., $\varphi(x' = 0) = 0$; $\varphi(x' = \eta) = V$ (Fig. 3), which can be written as

$$-\int_{w_{p^-} + w_n - \eta}^{w_{p^-} + w_n} \boldsymbol{E}\cdot d\boldsymbol{x} = \int_0^\eta E_x(x')dx' = V. \tag{25}$$

The local width η of the low-field domain $\mathcal{F}_l$ is given by (Figs. 1 and 2):

$$\eta(\boldsymbol{r}, t) = w_{p^-} + w_n - \xi(\boldsymbol{r}, t). \tag{26}$$

The injection level in the low-field domain $\mathcal{F}_l$ is assumed to be moderate: $n, p \approx N_a^-$. The carrier transport in this case is supported by the ambipolar drift mechanism which is described by the following partial differential equation for the excess concentrations $n = \Delta p$:

$$\frac{\partial n}{\partial t} = -(\boldsymbol{v}\cdot\nabla n) - \frac{n}{\tau_F}, \tag{27}$$

$$\boldsymbol{v} = -\frac{bN_a^-}{q[(b+1)n + N_a^-]^2}\cdot\boldsymbol{j} = -\frac{b+1}{b}\mu_p(a_h - a)\cdot\boldsymbol{E}. \tag{28}$$

Here $\boldsymbol{v}$ is the ambipolar drift velocity, τ_F is the carrier lifetime in the low-field domain, and $\boldsymbol{j}$ the three-dimensional current density vector defined by

$$\boldsymbol{j}=\sigma(j,j_n)\cdot\boldsymbol{E}, \tag{29}$$

where the local conductivity $\sigma(j,j_n)$ is assumed to be modulated due to the double injection of carriers into the field domain:

$$\sigma(j_n,j)=a_h\left[\frac{\sigma_{p^-}}{a_h-a(j_n,j)}\right], \tag{30}$$

with $\sigma_{p^-}=q\mu_p N_a^-$. The ratio

$$a(j_n,j)=\frac{j_n}{j} \tag{31}$$

denotes the electron fraction anywhere inside $\mathcal{F}_l$ including its boundaries with T_K and T_A [compare Eq. (12)].

When the modulation process of the carrier concentration—described by Eq. (27)—occurs, the plasma profile moves along the field lines with the drift velocity $\boldsymbol{v}$. For a p-type semiconductor the drift velocity $\boldsymbol{v}$ is directed from the cathode to the anode. The drift time through the whole width $l_F=\eta$ of the field domain $\mathcal{F}$ is $\tau_{dr}=l_F/|\boldsymbol{v}|$, and is assumed to be much shorter than the high-injection lifetime τ in the p^- bulk.

D. Final set of model equations

From the considerations above a characteristic time-scale hierarchy follows

$$\tau\gg\theta>\tau_1, \quad \tau_F\gg\tau_{dr}. \tag{32}$$

All values in Eq. (32) are much larger than the times for recharging the barrier and the diffusion capacitance of junction J_1 [given by $\tau_{1B}=r_{1n}^{em}C_B\sim 10$ ns and $\tau_{1D}=r_{1n}^{em}C_D=\theta_1\sim 1$ ns, respectively, where $r_{1n}^{em}=(dj_{1n}/d\varphi_1)^{-1}$] and the Maxwell relaxation time in the p^- bulk ($\tau_M=\epsilon\epsilon_0/\sigma_{p^-}<1$ ns).

The most inertial subsystem is therefore the anode transistor T_A due to the slow dynamics of the plasma charge in the virtual $\mathcal{P}$ base, which is described by

$$\frac{\partial Q}{\partial t}=D_\perp\Delta_\perp Q-\frac{Q}{\tau}+j_{\xi n}-j_{lk}. \tag{33}$$

As the electron transit time θ_1 in the cathode transistor T_K is much smaller than the carrier lifetime τ_1 in the p^+ base under low injection conditions, the base transport coefficient $\beta_n\approx 1/\cosh(\sqrt{2\theta_1/\tau_1})\approx 1$, so that $j_{Cn}=\alpha_1(j_1)j_1\simeq\gamma_1 j_1$. Because of the hierarchy of the time scales, Eq. (32), we consider Eq. (17) in the quasistatic approximation:

$$\sigma_1 w_p\Delta_\perp\varphi_1=j_1-j_C=j_{1p}-j_{Cp}, \tag{34}$$

where the latter equation is valid, since $\beta_n\approx 1$.

The electric field in the field domain is governed by the equation

$$\Delta\varphi=-\frac{\rho}{\varepsilon\varepsilon_0}, \tag{35}$$

with $\rho=qN_d$ in the n base and $\rho=0$ in the p^- bulk.

Neglecting the recombination term in Eq. (27) we describe the injection processes in $\mathcal{F}_l$ by

$$\frac{\partial n}{\partial t}=-(\boldsymbol{v}\cdot\boldsymbol{\nabla}n). \tag{36}$$

In addition to the x components of the electric field between $\mathcal{F}_h$ and $\mathcal{F}_l$ [Eq. (24)], all x components of the current densities at the internal boundaries x_0 between neighbored layers are continuous:

$$j_{x,\ldots}|_{x_0-0}=j_{x,\ldots}|_{x_0+0}. \tag{37}$$

At the side surfaces of the device, defined by $\{y=0,L_y\}$ and $\{z=0,L_z\}$, the field and diffusion current densities should vanish; therefore, the following boundary conditions have been chosen in all three subsystems (T_A, T_K, and the virtual collector):

$$(\boldsymbol{n}\cdot\boldsymbol{\nabla}_\perp Q)|_{y=0,L_y;\ z=0,L_z}=0, \tag{38}$$

$$(\boldsymbol{n}\cdot\boldsymbol{\nabla}_\perp\varphi_1)|_{y=0,L_y;\ z=0,L_z}=0, \tag{39}$$

$$(\boldsymbol{n}\cdot\boldsymbol{\nabla}_\perp\varphi)|_{y=0,L_y;\ z=0,L_z}=0. \tag{40}$$

Here $\boldsymbol{n}$ is a unit vector normal to the side surface.

It should be noted that condition (25) should also be satisfied for any vertical cross section of the device. In the following, global excitation of the device is considered to be controlled by a current source (i.e., $R\to\infty$ in Fig. 1):

$$\int_0^{L_y}\int_0^{L_z}j(y,z)\,dy\,dz=I=\text{const}, \tag{41}$$

where I is the total current in the external circuit.

The set of partial differential equations (33)–(36) together with the constraints (11)–(16), (18)–(20), (25), (28)–(30) and the boundary conditions (24) and (37)–(41) presents a self-consistent (1×2)-dimensional description of the multilayered device under study.

IV. STATIONARY HOMOGENEOUS STATES

Stationary plasma/field distributions, which are homogeneous with respect to the y-z plane, are described by a reduced set of equations for all space- and time-dependent variables $\mathbf{Y}$, and are obtained from Eqs. (33)–(36) by putting $\partial\mathbf{Y}/\partial t=0$, $\partial\mathbf{Y}/\partial\boldsymbol{y}=0$, and $\partial\mathbf{Y}/\partial\boldsymbol{z}=0$. As the electric field E and the current densities in the domain become strictly one dimensional, the ambipolar drift equation (36) can be reduced to

$$v_x\frac{\partial n}{\partial x}=0, \tag{42}$$

where v_x is the x component of the drift velocity $\boldsymbol{v}$. This means that the excess plasma concentration is constant any-

where in $\mathcal{F}_l$: $n=n_0$. Its value is defined by the ratio $j_n(x'=0)/j(x'=0)$ at the cathode-side boundary of the domain,

$$n_0=\Delta p_0=\frac{1}{b+1}\frac{\alpha_1}{a_h-\alpha_1}N_a^-,$$

where we have used the fact that for stationary homogeneous states the conductivity σ_0 of the domain $\mathcal{F}_l$ and the electric field E_0 itself are also determined by the ratio $j_n(x'=0)/j(x'=0)$:

$$\sigma_0(j,\alpha_1)=a_h\frac{\sigma_{p^-}}{a_h-\alpha_1}, \tag{43}$$

$$E_0(j,\alpha_1)=\frac{1}{\sigma_0(j,\alpha_1)}j. \tag{44}$$

For $\alpha_1\approx 0.5$–0.6 the excess concentration $n=\Delta p\approx N_a^-$, which is consistent with the assumption of moderate injection.

The width of the plasma layer ξ can be determined by solving Eq. (33) for the stationary state using $j_{\xi n}=\alpha_1 j$. For any arbitrary case with $\nu<1$ and $\mu>1$, the following transcendental equation for the normalized variable $\overline{\xi}=\xi/L_h$ can be derived:

$$\overline{\xi}^2+\left(\frac{j_\nu}{g_0\cdot j}\right)^{1-\nu}\overline{\xi}^\nu+\left(\frac{g_0\cdot j}{j_\mu}\right)^{\mu-1}\overline{\xi}^\mu-\overline{\xi}_0^2=0, \tag{45}$$

where

$$j_\nu=2\left[C_{sb}^{(\nu)}\left(\frac{\tau}{D_h}\right)^{\nu/2}\right]^{1/(1-\nu)},$$

$$j_\mu=2\left[C_{sp}^{(\mu)}\left(\frac{\tau}{D_h}\right)^{\mu/2}\right]^{1/(1-\mu)},$$

$$\overline{\xi}_0=\sqrt{\frac{2\alpha_1(j)}{g_0}},$$

and $g_0=g_0(\alpha_1)=a_h-\alpha_1$ is the one-dimensional limit value of g.

The $j(V)$ characteristic of the device for stationary homogeneous states is implicitly given by

$$V(j,\varphi_1)=V_{\mathcal{F}_h}+V_{\mathcal{F}_l}, \tag{46}$$

$$V_{\mathcal{F}_h}=V_{pth}+E_0(j,\alpha_1)w_n, \tag{47}$$

$$V_{\mathcal{F}_l}=E_0(j,\alpha_1)[w_{p^-}-\xi(j)], \tag{48}$$

where $V_{\mathcal{F}_l}$ and $V_{\mathcal{F}_h}$ denote the voltage drops across the low- and high-field domains, respectively, and $j=j(\varphi_1)$ and $\alpha_1=\alpha_1(\varphi_1)$ are determined by Eqs. (18)–(20).

The differential resistance r_d of the entire device follows from Eq. (46) as

$$r_d=\left.\frac{dV}{dj}\right|_0=\frac{\partial V}{\partial j}+\frac{\partial V}{\partial\alpha_1}\frac{d\alpha_1}{dj}+\frac{\partial V}{\partial\xi}\frac{d\xi}{dj}, \tag{49}$$

and depends on the respective nonlinearities of the injection current densities in T_K and T_A, which differ qualitatively from each other. The ratio $j_n(j)/j$, which increases monotonically with j, leads directly to a modulation of the bulk conductivity inside $\mathcal{F}_l$, resulting in a decrease in the field strength E_0 and the voltage $V_{\mathcal{F}_l}$. This causes an increase in the ratio $j_p(j)/j$ in T_A, which in turn leads to an increase in ξ and, consequently, to a decrease in $V_{\mathcal{F}_l}$. As is obvious from the definition of r_d [Eq. (49)], r_d may change with the current in different ways. In particular, branches with NDR can occur in the $j(V)$ characteristic. Since $V_{\mathcal{F}_h}$ depends on j, the existence of the n layer influences the boundaries of the NDR range to a certain though small degree.

We briefly consider two limit cases allowing an explicit analysis. For constant j_{sb} (which formally can be achieved by setting $\nu=0$) and $\mu=2$, Eq. (45) can be reduced to

$$\xi(\varphi_1,j(\varphi_1))=L_h\sqrt{\frac{2}{g_0}\left[\frac{\alpha_1(\varphi_1)-j_{sb}/j}{1+g_0 j/j_F}\right]}, \tag{50}$$

where a normalization factor $j_F=j_{\mu=2}=qN_a^+\lambda_{eff}/(b+1)\tau$ for Fletcher's leakage mechanism[38] has been introduced, and $j_{sb}=j_{\nu=0}/2=\text{const}$. As fas as the approximation for Fletcher's term in Eq. (50) is valid for $j\ll j_F$, the term $\sim j/j_F$ can also be neglected for estimations.

In the case that the sublinear leakage in T_A is completely suppressed we can set $j_{sb}=0$ in Eq. (50) and obtain an expression which is the same derived ealier in Ref. 33. This case has been completely studied within the framework of a one-dimensional model,[33] including a numerical analysis of the resulting $j(V)$ characteristics and the conditions for NDR occurence.

In the opposite limit case, when the injection properties in T_K are assumed to be linear, i.e., $\alpha_1=\text{const}$, and the nonlinear injection properties in T_A are taken into account by the rough approximation $j_{sb}\simeq\text{const}$, the implicit dependence ξ on φ_1 in Eq. (50) vanishes and we obtain

$$\xi(j)\approx L_h\sqrt{\frac{2}{g_0}\left(\alpha_1-\frac{j_{sb}}{j}\right)}. \tag{51}$$

In this case the modulated conductivity of the low-field domain does not depend on j; thus the field is simply proportional to j, and the $j(V)$ characteristic can be written explicitly as

$$V(j)-V_{pth}=V_0^+-V_0^-,$$

$$V_0^+=\frac{j}{\sigma_0}(w_n+w_{p^-}), \tag{52}$$

$$V_0^-\approx\frac{jL_h}{\sigma_0}\sqrt{\frac{2}{g_0}\left(\alpha_1-\frac{j_{sb}}{j}\right)}.$$

The differential resistance then consists of positive and negative parts, r_d^+ and r_d^-, respectively,

$$r_d=r_d^++r_d^-, \tag{53}$$

with

$$r_d^+ = \frac{w_n + w_{p^-}}{\sigma_0},$$

$$r_d^- = -\frac{L_h\sqrt{2/g_0}}{\sigma_0}\left[\sqrt{(\alpha_1 - j_{sb}/j)} + \frac{j_{sb}/j}{2\sqrt{(\alpha_1 - j_{sb}/j)}}\right].$$

It is evident from Eq. (53) that $r_d \leqslant 0$ can be fulfilled in a certain current interval with $j > j_{sb}/\alpha_1$. For higher current densities r_d is getting positive in any case. It should be noted that for sufficiently high current-density values the width ξ saturates to the value $\xi = L_h\sqrt{2\alpha_1/g_0}$ and, consequently, the voltage becomes a linear function of the current density: $V(j) = (w_{p^-} - L_h\sqrt{2\alpha_1/g_0})j/\sigma_0$. That means that the upper branch with positive differential resistance (PDR) can occur in the $j(V)$-characteristic even without any superlinear leakage mechanism in T_A.

V. INHOMOGENEOUS FLUCTUATIONS

In this section we analyze the stability of stationary states, which are homogeneous in the y-z plane, with respect to small (1×2)-dimensional fluctuations of all space dependent variables. We use the same approach as in Ref. 34, linearizing all variables $Y(x,\boldsymbol{r},t)$ in the vicinity of a stationary state $Y|_{stat}$:

$$\mathbf{Y}(x,\boldsymbol{r},t) = \mathbf{Y}|_{stat} + \delta\mathbf{Y}(x,\boldsymbol{r},t). \tag{54}$$

The small variations $\delta\mathbf{Y}(x,\boldsymbol{r},t)$ should satisfy the same boundary conditions [Eq. (38)] as the variable $\mathbf{Y}(x,\boldsymbol{r},t)$. This yields

$$\delta\mathbf{Y}(x,\boldsymbol{r},t) = \delta\mathbf{Y}(x,k)\cos(\boldsymbol{kr})\exp(\zeta t). \tag{55}$$

Here $\delta\mathbf{Y}(x,k)$ is a local amplitude; $\boldsymbol{r} = \boldsymbol{y} + \boldsymbol{z}$; and the wave numbers k, k_y, and k_z are subjected to the conditions $k^2 = k_y^2 + k_z^2$, $k_y = m\pi/L_y$, and $k_z = n\pi/L_z$, with m and n being integers. The condition connecting $k = k_x$ and k_y, k_z results from Eq. (23) that requires that the potential fluctuations are proportional to $\sinh(k_x x)\cos(k_y y)\cos(k_z z) = \sinh(k_x x)\cos(\boldsymbol{kr})$, with $|k_x| = |k|$. Within the framework of our approach, the full (1×2)-dimensional treatment of $\delta\mathbf{Y}$ is necessary only for the virtual collector field domain $\mathcal{F}$. The local variables in the virtual transistor layers are averaged along the x direction; thus the corresponding fluctuations are two dimensional.

A. Fluctuations of the excess charge and current density in the transistor T_A

Applying the linearization procedure Eq. (55) to the charge balance in T_A yields

$$\left(\zeta + \frac{1}{\tau} + k^2 D_\perp + \frac{\partial j_{lk}}{\partial Q}\right)\delta Q = \delta j_{\xi n} - \frac{\partial j_{lk}}{\partial \xi}\frac{\partial \xi}{\partial \eta}\delta\eta. \tag{56}$$

For $\delta Q(\theta, j_\xi, g)$, from Eqs. (11) and (12) we obtain

$$\delta Q = Q\left[\frac{1}{\theta}\frac{d\theta}{d\xi}\frac{d\xi}{d\eta}\delta\eta + \frac{1}{j}\delta j_\xi - \frac{1}{a_h - \alpha_1}\delta a\right]. \tag{57}$$

Relations between the fluctuations δQ, δj_ξ, δa and $\delta\eta$ depend on the fluctuations inside the domain $\mathcal{F}$ and at its cathode-side boundary with T_K, and are determined in the following subsections.

B. Fluctuations of the current-density and potentials in the transistor T_K

Linearization of Eqs. (17)–(19) with respect to perturbations (55) yields the following relations between the electron and the total current-density at the cathode-side boundary of the field domain:

$$\delta j_{Cn} = a_C^k \delta j_C, \tag{58}$$

$$a_C^k = \frac{r_1^{em}/r_{1n}^{em}}{1 + r_1^{em}/r_1^k} \equiv \frac{\alpha_1 + j d\alpha_1/dj_1}{1 + r_1^{em}/r_1^k}, \tag{59}$$

where $r_1^k = 1/\sigma_1 w_p k^2$ can be interpreted as a k-dependent effective resistance of the p^+ base, and $r_1^{em} = 1/(dj_1/d\varphi_1)$ and $r_{1n}^{em} = 1/(dj_{1n}/d\varphi_1)$ denote the differential resistance of the junction J_1 with respect to the total current density and its electron contribution, which depend parametrically on φ_1 [see Eqs. (18) and (20)].

C. Fluctuations of the potential, current density and boundary position in the field domain

A three-dimensional description of the potential, carrier concentration, and current-density fluctuations is rather complex. However, in the vicinity of the stationary homogeneous states, for which the relations $\boldsymbol{E} = -\boldsymbol{\nabla}\varphi = \text{const}$ and $\boldsymbol{\nabla} n = 0$ are valid, it can be simplified.

The ambipolar drift equation for concentration fluctuations in the low-field domain reduces to

$$\frac{\partial \delta n}{\partial t} = -\boldsymbol{v}|_0 \cdot \boldsymbol{\nabla}\delta n, \tag{60}$$

where the index 0 refers to stationary homogeneous solutions. The variable $\boldsymbol{v}|_0 = (v_0, 0, 0)$ is parallel to the x axis and constant along $\mathbf{x}$, while its absolute value depends on the stationary state under investigation. Using Eq. (55), from Eq. (60) we obtain

$$\zeta\delta n = -v_0\frac{d}{dx'}\delta n,$$

with the solution

$$\delta n = \delta n(x' = 0)\exp\left(-\frac{\zeta}{v_0}x'\right).$$

For sufficiently slow processes (the characteristic time scale of the fluctuation is $\sim 1/\zeta \gg \tau_{dr} \sim 0.1\ \mu\text{s}$) this means that the fluctuations of both the concentration δn and the local con-

ductivity $\delta\sigma$ in $\mathcal{F}_l$ are actually determined only by the current density fluctuations δj_C and δj_{Cn} in T_K and do not depend on the x-coordinate.

The fluctuations of the electron and the total current density in $\mathcal{F}_l$ again depend in different ways on both the conductivity modulation and the three-dimensional potential deformations. From Eqs. (29)–(31) we obtain

$$\delta \boldsymbol{j}_n = \delta(a \cdot \boldsymbol{j}) = \boldsymbol{j}_0 \cdot \delta a + \alpha_1 \cdot \delta \boldsymbol{j}, \tag{61}$$

$$\delta \boldsymbol{j} = \boldsymbol{E}_0 \cdot \delta\sigma + \sigma_0 \cdot \delta \boldsymbol{E}, \tag{62}$$

with $\alpha_1 = a_0$.

Evaluating Eq. (31) at the collector junction, $x = x_C$, and using Eq. (58) and the variational derivative of Eq. (30), we obtain

$$\delta a = \frac{1}{j_0}(\delta j_{Cn} - \alpha_1 \delta j_C) = \frac{1}{j_0}(a_C^k - \alpha_1)\delta j_C, \tag{63}$$

$$\delta\sigma = \frac{\sigma_0}{g_0}\delta a(j, j_n) = \frac{1}{j_0}\frac{\sigma_0}{g_0}(a_C^k - \alpha_1)\delta j_C. \tag{64}$$

Equation (61) then can be rewritten as

$$\delta \boldsymbol{j}_n = (a_C^k - \alpha_1) \cdot \frac{\boldsymbol{j}_0}{j} \cdot \delta j_C + \alpha_1 \cdot \delta \boldsymbol{j}, \tag{65}$$

connecting the current density fluctuations $\delta \boldsymbol{j}_n$, δj_C, and $\delta \boldsymbol{j}$.

Varying Eq. (22) we describe fluctuations of the electric field by three-dimensional potential fluctuations inside $\mathcal{F}_l$:

$$\delta \boldsymbol{E} = -\boldsymbol{\nabla}\,\delta\varphi. \tag{66}$$

Figure 3 shows how the potential fluctuation $\delta\varphi(x', \boldsymbol{r})$ leads to a perturbation of the floating anode-side boundary $\delta\eta$. The allowed fluctuations with the wave-number $k, k^2 = k_y^2 + k_z^2$, satisfying the Laplace equation (23) with the boundary conditions (38) have the form:

$$\delta\varphi(x', \boldsymbol{r}, t) = \delta\varphi_m \frac{\sinh(kx')}{\sinh(k\eta)}\cos(\boldsymbol{kr})\exp(\zeta t), \tag{67}$$

with the amplitude $\delta\varphi_m$. It should be noted that by the transformation $x' = w_{p^-} + w_n - x$ the x component of the electric field changes sign: $E_x = +\partial\varphi/\partial x'$ [compare Eq. (22)].

A relation between the fluctuation $\delta\eta$ and $\delta\varphi$ for $k \neq 0$ can be derived from condition (25),

$$\begin{aligned} V &= -\int_{w_{p^-}+w_n-\eta}^{w_{p^-}+w_n} \boldsymbol{E}\,d\boldsymbol{x} \\ &= \int_0^{\eta_0+\delta\eta} E_x\,dx' \\ &= E_0\eta_0 + E_0\delta\eta + \delta\varphi(x' = \eta_0), \end{aligned} \tag{68}$$

which leads to

$$\delta\eta(\boldsymbol{r}) = -\frac{1}{E_0}\delta\varphi(x' = \eta_0, \boldsymbol{r}). \tag{69}$$

The x component of the field fluctuation is proportional to the fluctuation of the floating boundary position $\delta\eta$:

$$\delta E_x = -kE_0\frac{\cosh(kx')}{\sinh(k\eta_0)}\delta\eta. \tag{70}$$

Equations (61) and (62) yield the fluctuations of the x component of the electron and the total current density, δj_{Cn} and δj_C, respectively, at the boundary between $\mathcal{F}$ and T_K:

$$\delta j_C = \frac{a_h - \alpha_1}{a_h - a_C^k}\frac{(-j_0 k)}{\sinh(k\eta_0)}\delta\eta, \tag{71}$$

$$\delta j_{Cn} = \frac{a_C^k(a_h - \alpha_1)}{a_h - a_C^k}\frac{(-j_0 k)}{\sinh(k\eta_0)}\delta\eta. \tag{72}$$

Similarly, it follows for the corresponding current density fluctuations $\delta j_{\xi n}$ and δj_ξ at the boundary between $\mathcal{F}$ and T_A:

$$\delta j_\xi = \left[\frac{a_C^k - \alpha_1}{a_h - a_C^k} + \cosh(k\eta_0)\right]\frac{(-j_0 k)}{\sinh(k\eta_0)}\delta\eta, \tag{73}$$

$$\delta j_{\xi n} = \left[\frac{a_h(a_C^k - \alpha_1)}{a_h - a_C^k} + \alpha_1\cosh(k\eta_0)\right]\frac{(-j_0 k)}{\sinh(k\eta_0)}\delta\eta. \tag{74}$$

Combining Eqs. (69) and (73), we can define an effective k-dependent differential resistance r_A^k,

$$r_A^k = \left[\left(\frac{a_C^k - \alpha_1}{a_h - a_C^k} + \cosh(k\eta_0)\right)\frac{\sigma_0 k}{\sinh(k\eta_0)}\right]^{-1}, \tag{75}$$

connecting the fluctuations δj_ξ and $\delta\varphi(x' = \eta_0)$:

$$\delta j_\xi = \frac{1}{r_A^k}\delta\varphi(x' = \eta_0).$$

The differential resistance r_A^k does not only depend on the strength of the three-dimensional potential deformation for a given wave-number k (as in the case discussed in Ref. 34), but additionally depends on the conductivity modulation determined by both homogeneous and nonuniform fluctuations in T_K, which is reflected in the dependence of r_A^k on the coefficients α_1, σ_0, and a_C^k.

The shape of the electric-field fluctuations in the field domain can be illustrated by considering the differential quotient of the coordinates y_E and x_E and assuming a uniform distribution along the z direction, i.e., $k = k_y$:

$$\frac{dy_E}{dx_E} = \frac{\delta E_y(x_E, y_E)}{\delta E_x(x_E, y_E)} = \left(\frac{\partial\delta\varphi}{\partial y}\right) \Big/ \left(\frac{\partial\delta\varphi}{\partial x}\right). \tag{76}$$

With $x' = w_{p^-} + w_n - x$ the solution $y_E(x')$ of Eq. (76) is given by

$$\sin(ky_E)\cosh(kx_E') = C, \tag{77}$$

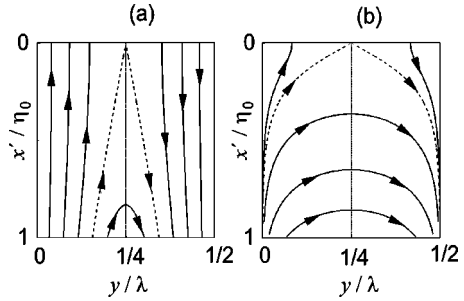

FIG. 4. Current-density lines in the field domain for fluctuations with two different wavelengths, $\lambda \gg \eta_0$ (a) and $\lambda \approx \eta_0$ (b).

where C is an integration constant. By using Eqs. (62) and (67) we obtain the following equation determining the vector lines of the current density fluctuations:

$$\frac{dy_j}{dx_j'} = \frac{\delta j_y(x_j', y_j)}{\delta j_x(x_j', y_j)} = \frac{\sigma_0 \partial \delta\varphi/\partial y}{E_0 \delta\sigma + \sigma_0 \partial \delta\varphi/\partial x'}. \tag{78}$$

The solution of this equation is

$$\sin(k y_j)\left[\cosh(k x_j') + \frac{a_C^k - \alpha_1}{a_h - a_C^k}\right] = C. \tag{79}$$

The curves defined by $y_E(x_E', C)$ and $y_j(x_j', C)$ can be interpreted as contour lines for different constants C and surfaces defined by Eqs. (77) and (79). Figure 4 shows the current-density lines for two cases with $\lambda/\eta_0 \gg 1$ and $\lambda/\eta_0 \approx 1$, where $\lambda = 2\pi/k$. The different current-density lines have been obtained by varying C in Eq. (79). When $\lambda/\eta_0 \gg 1$ [Fig. 4(a)], the current flow in the field domain is mainly parallel to the x direction and most of the current-density lines starting at the anode-side boundary of the field domain ($x' = \eta_0$) arrive at the cathode-side boundary ($x' = 0$) and enter T_K; that means the contour plot of the current-density lines for fluctuations with a sufficiently small wave number k differs only slightly from that of the homogeneous flow. In contrast to this, most of the current-density lines do not enter T_K when the wavelength $\lambda = 2\pi/k$ is of the same order as η_0 [Fig. 4(b)]. In this case we can not expect that the corresponding current-density fluctuation is noticeably amplified by T_K, and r_A^k [Eq. (75)] is approximately given by $\eta_0/(2\pi\sigma_0)$.

D. Dispersion relation

Eliminating the amplitudes $\delta\mathbf{Y}$ from Eqs. (56), (57), (63), and (71)–(74), we find the dispersion relation $\zeta(k)$,

$$\zeta(k) = -k^2 D_\perp + \zeta_G(k) - \zeta_{sp}(k) - \zeta_{sb}(k), \tag{80}$$

where the components are given by

$$\zeta_G(k) = \left[\frac{B_1(k)}{B_2(k)} - 1\right]\frac{1}{\tau}, \tag{81}$$

$$B_1(k) = \alpha_1 + a_h\left(\frac{a_C^k - \alpha_1}{a_h - a_C^k}\right)\frac{1}{\cosh(k\eta)},$$

$$B_2(k) = \frac{g_0}{2}\left(\frac{\xi}{L_h}\right)^2\left[1 + \frac{2\tanh(k\eta)}{k\xi}\right] > 0,$$

$$\zeta_{sp}(k) = \mu\frac{j_{sp}}{Q}\left[1 - \frac{1}{k\xi\coth(k\eta) + 2}\right] > 0, \tag{82}$$

$$\zeta_{sb}(k) = \nu\frac{j_{sb}}{Q}\left[1 - \frac{1}{k\xi\coth(k\eta) + 2}\right] > 0, \tag{83}$$

and the values of ξ, η, and Q belong to the stationary homogeneous state under investigation as determined in Sec. IV. In what follows we investigate the stability characteristics of stationary homogeneous states with respect to fluctuations with a wave number k by evaluating Eqs. (81)–(83).

VI. STABILITY ANALYSIS

A. Limit cases

As is evident from Eqs. (80) and (81), $\zeta(k)$ can become only positive if $\zeta_G(k)$ is sufficiently large. Besides the obvious dependence on the strength of the regeneration process between T_A and T_K, it is influenced by a damping mechanism, caused by the transversal diffusion in T_K, and a destabilizing mechanism emanating from deformations of the homogeneous field distribution inside the field domain $\mathcal{F}$. To illuminate the influence of the different mechanisms on $\zeta_G(k)$ we study two special cases in more detail.

1. Stabilizing influence of transversal currents in T_K and T_A

The influence of transversal currents in T_K on the stability behavior can be illustrated by ignoring the fluctuations of the field domain. Then B_1 in Eq. (81) reduces to

$$\alpha_1 + a_h\frac{j d\alpha_1/dj - \alpha_1 r_1^{em}/r_1^k}{g_0 - j d\alpha_1/dj + a_h r_1^{em}/r_1^k}.$$

Evaluating Eq. (81) for small wave-numbers k and small η, $\zeta_G(k)$ depends parabolically on k:

$$\zeta_G(k) = -D_{\varphi_1}k^2 + \zeta_{G0}, \tag{84}$$

$$D_{\varphi_1} = \frac{a_h g_0(\alpha_1 + j d\alpha_1/dj) r_1^{em}}{\tau(g_0 - j d\alpha_1/dj)^2 B_2(0)} q\mu_p N_a w_p, \tag{85}$$

$$\zeta_{G0} = \frac{1}{\tau}\left[\frac{\alpha_1 + (a_h j d\alpha_1/dj)/(g_0 - j d\alpha_1/dj)}{B_2(0)} - 1\right]. \tag{86}$$

The coefficient D_{φ_1} can be interpreted as an effective transversal diffusion coefficient of the potential of the p^+ base and ζ_{G0} is the increment of fluctuations at $k \to 0$.

Further simplification can be done when the superlinear electron leakage in T_A is due to Fletcher's mechanism, i.e., $\mu = 2$. Using Eq. (50) we obtain

$$B_2(k=0)=\frac{\alpha_1-j_{sb}/j}{1+g_0 j/j_F}\left(1+\frac{2\eta}{\xi}\right).$$

Taking into account $r_1^{em}\approx(kT/q)/j$ and using $D_h=2a_hD_p$, D_{φ_1} can be approximated by

$$D_{\varphi_1}\approx\frac{g_0(1+g_0 j/j_F)(\alpha_1+jd\alpha_1/dj)qN_a w_p D_h}{2\tau(g_0-jd\alpha_1/dj)^2(\alpha_1-j_{sb}/j)(1+2\eta/\xi)j}.$$

Inserting $B_2(0)$ into Eq. (86) yields

$$\zeta_{G0}=\left(\frac{g_0(\alpha_1+jd\alpha_1/dj)(1+g_0 j/j_F)}{(g_0-jd\alpha_1/dj)(\alpha_1-j_{sb}/j)(1+2\eta/\xi)}-1\right)\frac{1}{\tau}.$$

For realistic parameters $D_{\varphi_1}\approx(3\ldots10)D_h$. The sign of ζ_{G0} depends on the sign of the differential resistance r_d.

For larger values of k, we have $r_1^{em}/r_1^k\gg1$, the nominator $B_1\to0$ and $\zeta_G(k)$ saturates: $\zeta_G(k)\to(-1/\tau)$. As for the transistor T_A, the term

$$\zeta_{D_\perp}=-k^2D_\perp,\quad D_\perp\sim D_h,$$

is apparently the only stabilizing factor.

2. Destabilizing influence of the field domain $\mathcal{F}$

For small and large wave numbers k of the potential fluctuations in the field domain $\mathcal{F}$ we neglect the ''potential diffusion'' in T_K by supposing $\sigma_\perp=\sigma_1 w_p=0$, i.e., by suppressing transversal currents in the p^+ base. For simplicity, α_1 is assumed to be constant and, as in the previous subsection, the superlinear electron leakage in T_A is assumed to be caused by Fletcher's mechanism ($\mu=2$). Then $\zeta_G(k)$ is given by

$$\zeta_G(k)=\frac{1}{\tau}\left[\frac{\alpha_1(1+g_0 j/j_F)}{(\alpha_1-j_{sb}/j)[1+2\tanh(k\eta)/(k\xi)]}-1\right]. \tag{87}$$

For small values of k we have

$$\zeta_G(k)\approx+k^2D_F+\zeta_{G0}, \tag{88}$$

$$D_F=\frac{2}{3\tau}\frac{\alpha_1(1+g_0 j/j_F)}{(\alpha_1-j_{sb}/j)}\frac{\eta^3}{\xi(1+2\eta/\xi)^2}, \tag{89}$$

$$\zeta_{G0}=\frac{1}{\tau}\left[\frac{\alpha_1(1+g_0 j/j_F)}{(\alpha_1-j_{sb}/j)(1+2\eta/\xi)}-1\right]. \tag{90}$$

The parameter D_F can be interpreted as a transversal diffusion coefficient of the potential fluctuations in the field domain at small k, and $1/\zeta_{G0}$ is the characteristic time scale for the damping (or undamping) of transversally uniform potential fluctuations $k=0$. It should be noted that Eq. (86) describing the evolution of uniform fluctuations in the cathode transistor (Sec. VI A 1) reduces to Eq. (90) for $\alpha_1=$const.

At very large values of k the function $\zeta_G(k)$ saturates slowly according to

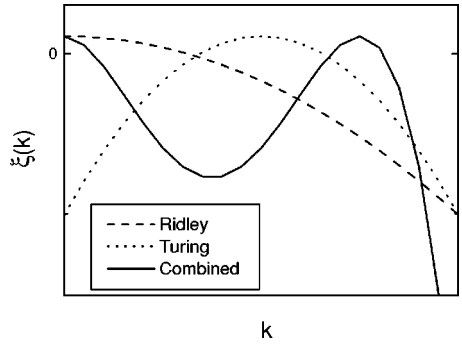

FIG. 5. Schematic plot of the three characteristic cases showing how the dispersion relation $\zeta(k)$ may become positive. The three cases can be attributed to a Ridley-type instability (dashed line), a Turing-type instability (dotted line), and the simultaneous appearance of Ridley- and Turing-type of instabilities (solid line).

$$\zeta_G(k)\to\frac{1}{\tau}\left(\frac{\alpha_1(1+g_0 j/j_F)}{(\alpha_1-j_{sb}/j)[1+2/(k\xi)]}-1\right).$$

Equations (87)–(89) illustrate how the damping influence of the domain is reduced and the transversal ''potential diffusion'' in the field domain may destabilize the homogeneous state. It is noteworthy that the potential fluctuations are amplified by the static value of the current gain α_1 and this kind of amplification cannot take place under the conditions studied in Ref. 34.

3. Hierarchy of transversal coupling mechanisms

For realistic design parameters the diffusion coefficient D_{φ_1} is of the order of 50–100 cm^2/s, while the value of D_F is about $\sim$10–20 cm^2/s for $j_{sb}=0$ and may reach several tens of cm^2/s for appropriately adjusted shunts of the anode emitter. There are two characteristic hierarchy sequences of the diffusion coefficients:

$$D_{\varphi_1}>D_\perp>D_F \tag{91}$$

or

$$D_{\varphi_1}>D_F>D_\perp. \tag{92}$$

In the first case one can expect ζ to decrease monotonously with k, because the two leading terms $-k^2(D_{\varphi_1}+D_\perp)$ are negative and $D_F(j)$ is small. In the second case a peculiar situation may occur, where $\zeta(k)$ decreases as $-k^2D_{\varphi_1}$ at small values of k, while it increases as $+k^2D_F$ at larger k values; finally at very large values of k the term $-k^2D_\perp$ is larger than all other contributions and $\zeta(k)$ becomes negative in any case.

Therefore, depending on the parameter combination, we can distinguish three characteristic ways of how $\zeta(k)$ can become positive with increasing current (Fig. 5): (i) at small k values, $0\leqslant k\ll k_{\max}$; (ii) only inside a certain k interval $0<k_{\min}\leqslant k\leqslant k_{\max}$; or (iii) there may appear two isolated ranges for k, where $\zeta(k)>0$. The first case can be identified with an instability of Ridley's type and the second with an instability of Turing's type, while in the third case both in-

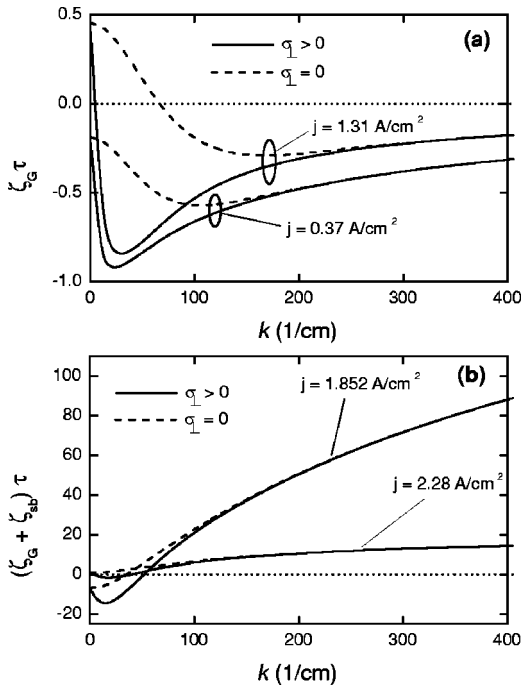

FIG. 6. (a) $\zeta_G(k)$ when the nonlinear injection properties of the cathode transistor are dominating with $j_{sb0}=1.5\times10^{-2}$ A/cm^2, $C_{sb}^{(\nu)}=C_{sp}^{(\mu)}=0$, and $\nu_1=0.125$. (b) Sum of $\zeta_G(k)$ and $\zeta_{sb}(k)$ when the nonlinear injection properties of the anode transistor are dominating with $j_{sb0}=0$, $\nu=0.125$, $\mu=2$, and $j_\nu=5$. Both diagrams $\sigma_\perp=\sigma_1 w_p=76.8$ mS>0 correspond to $N_a=5\times10^{18}$ cm^{-3}.

stabilities can occur simultaneously, which may lead to the evolution of complex spatiotemporal patterns.

It should be noted that the term ζ_{sp} acts at relatively large currents j (though $j\ll j_F$). The term ζ_{sb} is only slowly increasing with current and can be considered to be relatively small. Therefore, these two terms omitted above do not change the main conclusions of the qualitative analysis.

B. Numerical illustrations

In calculations we use the following values for physical constants: $q=1.6\times10^{-19}$ C, $k=1.38\times10^{-23}$ J/K, $\epsilon_0=8.854\times10^{-14}$ F/cm, $\epsilon(Si)=11.7$, $T=300$ K, $n_i=1.45\times10^{10}$ cm^{-3}, $\mu_p=480$ cm^2/Vs, $\mu_n=b\mu_p$, $b(Si)=2.8$, and $D_{n,p}=kT\mu_{n,p}/q$; the basic design parameters are given by $w_p=2\times10^{-4}$ cm, $w_n=0$, $w_{p^-}=5\times10^{-2}$ cm, $N_a^-=1\times10^{13}$ cm^{-3}, $N_a=5\times10^{17}$ cm^{-3}, $\tau=5$ μs, $j_{n0}=2\times10^{-11}$ A/cm^2, and $\mu=2$. The parameters of the anode contact p^+ layer are: $N_a^+=10^{19}$ cm^{-3} and $\lambda_{eff}=10^{-4}$ cm, leading to $j_F\approx8.4$ A/cm^2. The hole mobility in the p^+ base of the cathode transistor T_K has been reduced to $\mu_{p^+}=300$ cm^2/Vs.

The influence of the nonlinear injection properties of the cathode and the anode transistor on the dispersion relation $\zeta(k)$ are demonstrated in Fig. 6. For this purpose, either the anode emitter leakage current $j_{lk}=j_{sb}+j_{sp}$ [Fig. 6(a)] or the sublinear part of the cathode emitter leakage current density, j_{sub} [Fig. 6(b)], was assumed to be zero. The four curves in both diagrams represent the most interesting components of the dispersion relation for two current-density values and for two values of $\sigma_\perp$, respectively.

TABLE I. Parameter sets used for the calculations.

Set	j_{p0} (A/cm^2)	j_{sb0} (A/cm^2)	ν_1	ν
N1	0.952×10^{-11}	2×10^{-2}	0.1	0.25
N2	1.026×10^{-11}	5×10^{-4}	0.225	0.12

In Fig. 6(a) the nonlinear leakage currents j_{sb} and j_{sp} have been neglected so that the NDR is only due to the nonlinear injection properties of the cathode emitter. In this case, $\zeta(k)$ is simply given by the sum of $\zeta_G(k)$ and $-k^2D_\perp$. For a fixed current-density value the two $\zeta_G(k)$ curves for the two different $\sigma_\perp$ values merge together for large wave numbers, while $\zeta_G(k,\sigma_\perp>0)<\zeta_G(k,\sigma_\perp=0)$ for $k<250$ cm^{-1}. This clearly illustrates the stabilizing influence of current spreading inside the p^+ base ($\sigma_\perp>0$) for a certain k interval. Moreover it is evident that uniform fluctuations with $k=0$ are the most critical ones, leading to an instability of Ridley's type.

In Fig. 6(b) the sublinear part of the emitter leakage current density of the cathode transistor is set to zero, and α_1 is assumed to be independent of the current density, so that the NDR is based essentially on the nonlinear injection properties of the anode emitter. Since $\zeta_{sp}(k)$ is rather small in this case, the sum of only $\zeta_G(k)$ and $\zeta_{sb}(k)$ is shown in the diagram. Similar to Fig. 6(a), current spreading in the p^+ base tends to stabilize fluctuations at low k values. However, at larger wave numbers the destabilizing effect of potential fluctuations in the field domain comes to light, reflecting the dominance of a nonuniform fluctuation with a wave-number $0<k_{\min}<k<k_{\max}$ when a stationary uniform state is destabilized—similar to a Turing type of instability. Altogether it can be concluded that an instability of Ridley type is favored when the activity of T_K is high (at large $d\alpha_1/dj$), while an instability of Turing type preferrably occurs when the activity of T_A dominates. These circumstances can be used for controlling the structure properties.

The $j(V)$ characteristics may contain current density intervals with NDR or may show PDR in the whole investigated current density interval. In the following we consider two examples with NDR, showing a Ridley type of instability and an analog of the Turing instability. The design parameters are specified in Table I. In the two investigated cases the activities of the two transistors are comparable; however, for the parameter set N1, contributions of T_K where chosen to dominate slightly over T_A. For the second case (parameter set N2) the situation is the reverse.

The $j(V)$ characteristics calculated for different parameter values of j_ν are presented in Fig. 7. The traces $J_R(j_\nu)$ and $J_T(j_\nu)$ are built up by Ridley and Turing instability points, calculated for the corresponding $j(V)$ characteristics. These traces define regions where $\zeta(k)\geqslant0$. In Fig. 7(a) the two regions do not overlap, Turing's region is situated at smaller currents on the lower PDR branches of the $j(V)$-characteristics. In Fig. 7(b) the two regions overlap partly. At the intersection points M_{LEFT} and M_{RIGHT} of the traces J_T and J_R the value of both dispersion relations is

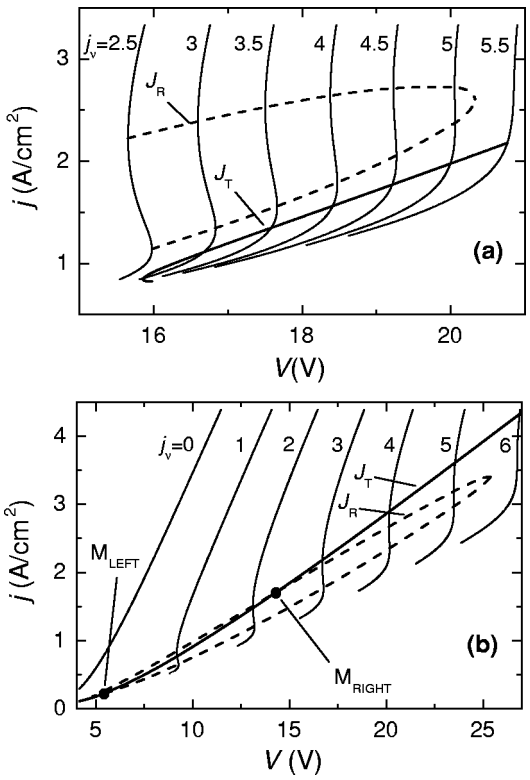

FIG. 7. $j(V)$ characteristics calculated for the two parameter sets N1 (a) and N2 (b). The traces $J_R(j_\nu)$ and $J_T(j_\nu)$ mark the stability border with respect to instabilities of Ridley and Turing types.

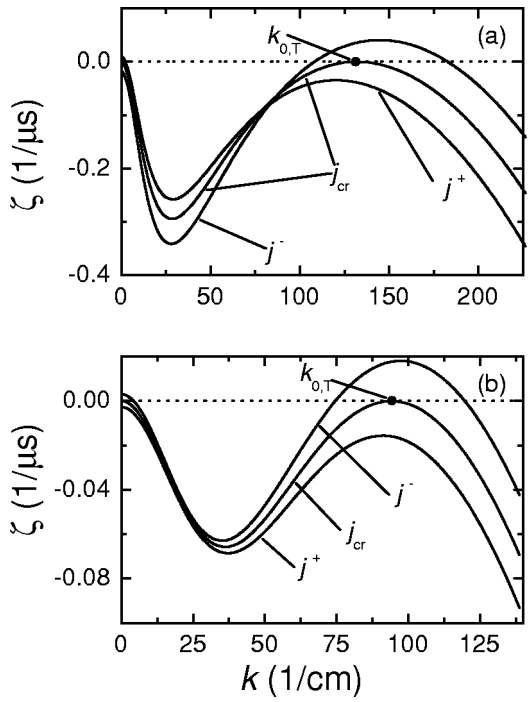

FIG. 8. Dispersion relations at the two intersection points M_{LEFT} (a) and M_{RIGHT} (b) of Fig. 7(b) for three different current densities, respectively.

zero, i.e. $\zeta(k_{0,R})=\zeta(k_{0,T})=0$ at a certain critical current-density value $j_{0,R}=j_{0,T}$ and at certain values of the wave numbers $k_{0,R}$ and $k_{0,T}$ which differ from each other.

The dispersion relations $\zeta(k)$ at the two intersection points are shown in Figs. 8(a) and 8(b), respectively, for three different current densities (j^-,j_{cr},j^+). In both cases $\zeta_{cr}(k)$ belonging to the critical current density j_{cr}, which has been determined together with the respective value of j_ν from Fig. 7, is negative for all wave numbers k up to but excluding two points $k=k_{0,R}=0$ and $k=k_{0,T}>0$. By varying the current density around j_{cr} the evolution of $\zeta(k)$ is qualitatively different in the two intersection points. At the point M_{LEFT} an increase in the current density up to j^+ causes an increase in ζ around $k=0$ and a decrease in ζ around $k=k_{0,T}$, i.e. intensifying Ridley's instability and stabilizing the device with respect to an instability of Turing type. As for the right intersection point M_{RIGHT}, both instability types are damped (intensified) as the current density increases (decreases). This is reflected in the dispersion relation by the fact that two narrow k bands arise where $\zeta(k)>0$ which are separated by a k-interval with $\zeta<0$.

When the device is operating in a state where the uniform state is unstable with respect to both Ridley and Turing types of instability, interesting spatial-temporal patterns might appear due to competition processes of different evolving fluctuations. For example, if initially perturbations with a long wavelength are predominating, so that a large area of the sample switches into the on state while another large area remains in the off state, this state itself might become unstable with respect to perturbations with small wavelengths and cause the evolution of periodic Turing patterns. These Turing patterns may evolve simultaneously, but in different ways for the two parts in the on- and off-states, respectively. Finally two transversal domains with different types of Turing patterns could appear, raising questions concerning their mutual interaction and possible coexistence. Many other scenarios based on these instabilities and leading to interesting self-organized structures are conceivable.

In this context it is interesting to note that the dispersion relation in the case of coinciding Ridley and Turing instabilities looks similar to the real part of the dispersion relation near the codimension-two Turing-Hopf bifurcation studied in a semiconductor heterostructure model.[41] In such a system complex spatiotemporal patterns consisting of mixed Turing-Hopf modes may appear, as has been shown for systems with one-[41] and two-dimensional[42] contact geometries. Analogous to these results, in our case we expect a complex behavior, in the form of mixed patterns, consisting of filamentary and periodical current-density distributions. However, the set of model equations studied in Refs. 41 and 42 contains only lateral degrees of freedom. The relevant vertical (along the **x** direction) processes are reflected in local kinetic functions. The instabilities in our system are essentially governed by an interaction between the stabilizing processes in the anode and the cathode transistor, and the destabilizing influence of the field domain in between. For this reason the full (1×2)-dimensional description is necessary in contrast to the mentioned semiconductor heterostructure, where local kinetic functions are used to account for the vertical processes.

Finally let us turn attention to the approximations used at the setting of the initial problem. For the current-density interval of interest for the appearance of instabilities, $j \sim 1-10$ A/cm^2, the typical voltage drop across the sample amounts to a few tens of volts, and is therefore distinctly larger than the voltage drops across the emitter junctions as was supposed. The width ξ of the $\mathcal{P}$ layer is typically in the range of $\xi=(0.05-0.2)w_{p^-}$ for the investigated cases with NDR, so ξ is small in comparison with the width $l_F=\eta$ of the field domain. The transient time through the width ξ is equal to $\theta=\xi^2/2D_h=(1-2)$ μs, and the drift time for the field domain is $\tau_{dr}=(0.1-0.5)$ μs. Therefore, the condition $\tau \gg \theta \gg \tau_{dr}$ is fulfilled which justifies the corresponding assumptions chosen in Secs. II and III.

VII. SUMMARY

A detailed analysis of the field punch-through mode in p^+-p^--n-p^+-n^{++} structures has been presented in the frame of a two-transistor model where the two transistors are coupled by a high-field region. It turned out that depending on the nonlinear injection properties of the emitter regions in the two transistors, instabilities of Ridley or Turing type may destabilize uniform current-density states. In particular, we have shown that Ridley and Turing instabilities may also appear simultaneously under certain conditions. The interaction and competition of the different fluctuations evolving simultaneously or in a secondary bifurcation may lead to interesting types of patterns with complex or even unexpected spatiotemporal behaviors.

ACKNOWLEDGMENTS

The present paper was prepared within the framework of the international project ''Dissipative Pattern Formations in Semiconductors and Semiconductor Devices'' supported by the Deutsche Forschungsgemeinschaft and the Russian Academy of Science.

[1] A. Turing, Philos. Trans. R. Soc. London, Ser. B **237**, 37 (1952).
[2] G. Nicolis and I. Prigogine, *Self-Organization in Non-Equilibrium Systems* (Wiley, New York, 1977).
[3] H. Haken, *Advanced Synergetics*, 2nd ed. (Springer, Berlin, 1987).
[4] B. Kerner and V.V. Osipov, *Autosolitons* (Kluwer, Dordrecht, 1994).
[5] *Evolution of Structures in Dissipative Continuous Systems*, edited by F.H. Busse and S.C. Müller (Springer, Berlin, 1998).
[6] D. Ruwisch, M. Bode, H.-J. Schulze, and F.-J. Niedernostheide, in *Nonlinear Physics of Complex Systems*, edited by J. Parisi, S. Müller, and W. Zimmermann, Lecture Notes in Physics, Vol. 476, (Springer, Berlin, 1996), pp. 194–212.
[7] M. Bode, J. Fischer, O. Freyd, F.-J. Niedernostheide, and H.-J. Schulze, Artificial Intelligence **130/1**, 75 (2001).
[8] C.V. Radehaus and H. Willebrand, in *Nonlinear Dynamics and Pattern Formation in Semiconductors and Devices*, edited by F.-J. Niedernostheide (Springer, Berlin, 1995), pp. 250–265.
[9] R. Buczynski, V. Baukens, T. Szoplik, A. Goulet, N. Debaes, A. Kirk, P. Heremans, R. Vounckx, I. Veretennicoff, and H. Thienpont, IEEE Photon. Technol. Lett. **11**, 367 (1999).
[10] B.S. Kerner and V.S. Sinkevich, Pis'ma Zh. Éksp. Teor. Fiz. **36**, 359 (1982) [JETP Lett. **36**, 436 (1982)].
[11] K.M. Mayer, R. Gross, J. Parisi, J. Peinke, and R.P. Huebener, Solid State Commun. **63**, 55 (1987).
[12] J. Hirschinger, F.-J. Niedernostheide, W. Prettl, and V. Novák, Phys. Rev. B **61**, 1952 (2000).
[13] E. Schöll, *Nonlinear Spatio-Temporal Dynamics and Chaos in Semiconductors* (Cambridge University Press, Cambridge 2001).
[14] K. Aoki, *Nonlinear Dynamics and Chaos in Semiconductors* (Institute of Physics, Bristol, 2000).
[15] K.M. Mayer, J. Peinke, B. Röhricht, J. Parisi, and R. Huebener, Phys. Scr. **T19**, 505 (1987).
[16] V.A. Vashchenko, B.S. Kerner, V.V. Osipov, and V.F. Sinkevich, Fiz. Tekh. Poluprovodn. **24**, 1705 (1990) [Sov. Phys. Semicond. **24**, 1065 (1990)].
[17] R. Symanczyk, E. Pieper, and D. Jäger, Phys. Lett. A **143**, 337 (1990).
[18] F.-J. Niedernostheide, M. Arps, R. Dohmen, H. Willebrand, and H.-G. Purwins, Phys. Status Solidi B **172**, 247 (1992).
[19] F.-J. Niedernostheide, B.S. Kerner, and H.-G. Purwins, Phys. Rev. B **46**, 7559 (1992).
[20] J. Oetjen, R. Jungblut, U. Kuhlmann, J. Arkenau, and R. Sittig, Solid-State Electronics **44**, 117 (2000).
[21] N.A. Vlasenko, Z.L. Denisova, L.I. Veligura, S. Zuccaro, F.-J. Niedernostheide, and H.-G. Purwins, J. Cryst. Growth **214/215**, 944 (2000).
[22] S. Zuccaro, F.-J. Niedernostheide, B. Kukuk, M. Strych, and H.-G. Purwins, Phys. Rev. E **62**, 1284 (2000).
[23] B.K. Ridley, Proc. Phys. Soc. London **82**, 954 (1963).
[24] A.V. Gorbatyuk, I.A. Linijchuk, and A.V. Svirin, Pis'ma Zh. Tekh. Fiz. **15**, 42 (1989) [Sov. Tech. Phys. Lett. **15**, 224 (1989)].
[25] A.V. Gorbatyuk and P.B. Rodin, Pis'ma Zh. Tekh. Fiz. **16**, 89 (1990) [Sov. Tech. Phys. Lett. **16**, 519 (1990)].
[26] A.V. Gorbatyuk and P.B. Rodin, Radiotekh. Elektron. **40**, 1876 (1994) [J. Commun. Technol. Electron. **40**, 49 (1995)].
[27] A.V. Gorbatyuk and P.B. Rodin, Z. Phys. B: Condens. Matter **104**, 45 (1997).
[28] M. Meixner, P. Rodin, and E. Schöll, Phys. Rev. E **58**, 2796 (1998); **58**, 5586 (1998).
[29] F.-J. Niedernostheide and M. Kleinkes, Phys. Rev. B **59**, 7663 (1999).
[30] F.-J. Niedernostheide, M. Ardes, M. Or-Guil, and H.-G. Purwins, Phys. Rev. B **49**, 7370 (1994).
[31] F.-J. Niedernostheide, H.-J. Schulze, S. Bose, A. Wacker, and E. Schöll, Phys. Rev. E **54**, 1253 (1996).
[32] A. Wierschem, F.-J. Niedernostheide, A.V. Gorbatyuk, and H.-G. Purwins, Scanning **17**, 106 (1995).
[33] A.V. Gorbatyuk and F.-J. Niedernostheide, Physica D **99**, 339 (1996).

[34] A.V. Gorbatyuk and F.-J. Niedernostheide, Phys. Rev. B **59**, 13 157 (1999).
[35] W. Gerlach, *Thyristoren* (Springer, Heidelberg, 1981) (in German).
[36] S.M. Sze, *Physics of Semiconductor Devices* (Wiley, New York, 1981).
[37] B.J. Baliga, *Power Semiconductor Devices* (PWS, Boston, 1996).
[38] N.H. Fletcher, Proc. IRE **45**, 863 (1957).
[39] S.C. Choo, IEEE Trans. Electron Devices **19**, 954 (1972); Solid-State Electronics **16**, 197 (1973).
[40] See, e.g., A. Schenk, *Advanced Physical Models for Silicon Device Simulation* (Springer, New York, 1998).
[41] M. Meixner, A. De Witt, S. Bose, and E. Schöll, Phys. Rev. E **55**, 6690 (1997).
[42] W. Just, M. Bose, S. Bose, H. Engel, and E. Schöll, Phys. Rev. E **64**, 026219 (2001).